

# Electron solvation in methane and ethane

Zhihua Liu and Bruce J. Berne

*Department of Chemistry and Center for Biomolecular Simulation, Columbia University, New York, New York 10027*

(Received 22 June 1993; accepted 27 August 1993)

The solvation of excess electrons in fluid methane and ethane is studied by path integral Monte Carlo computer simulation and by the fast-Fourier-transform–Lanczos diagonalization method using a newly developed electron-alkane pseudopotential. Many-body polarization interactions between solvent molecules are treated using a mean field approximation in the simulation. In methane, it is found that the electron is in an extended state throughout the whole fluid density range studied. In ethane, it is found that the solvated electron gradually becomes localized or “self-trapped,” with cavity formation occurring at a fluid density where experimentally the electron is found to have a very low mobility and the threshold value for electron photoconduction rises above zero. The electronic ground state energies in the unperturbed solvent and in the electron-equilibrated solvent were compared. At the same density these electronic energies are very close to each other in methane and in the low density ethane fluids, but at higher ethane densities, where cavity formation takes place, the ground state energy in the electron solvated fluid is lower than that in the unperturbed fluid.

## I. INTRODUCTION

For several decades, the properties of excess electrons in a wide variety of fluids have been studied.<sup>1–5</sup> Experimental studies of the conduction and energetics of excess electrons have shown that alkane fluids can be subdivided into two distinctive classes depending on the molecular symmetry (geometry) of the solvent molecules. The electron mobility in branched alkanes (such as methane, isobutane, and neopentane) exhibit an anomalous behavior similar to that in the heavy rare gas fluids (Ar, Kr, Xe).<sup>1,2</sup> With increasing fluid density, the electron mobility first decreases to a minimum before reaching the critical density of the fluid and then rapidly rises to a maximum (in the liquid density regime) after which it decreases again. In straight chain molecules like the *n*-alkanes the electron mobility decreases almost monotonically with increasing fluid density. It was found that the more branched the molecule, the more pronounced is the anomalous electron mobility behavior. For example, the mobility maximum in neopentane is as high as the electron mobility in some semiconductors, while the electron mobility in *n*-pentane at the same fluid density is more than twenty times lower.<sup>6</sup> The effect of temperature on the mobility in chain and branched alkanes is also very different. In all the *n*-alkane liquids, the electron mobility exhibits an Arrhenius-type dependence on temperature with activation energies between 0.1 and 0.2 eV. In branched alkanes, however, much smaller activation energies were observed. This is especially apparent in spherically shaped molecules like methane, neopentane, and tetramethylsilane, where the electron mobility is independent of temperature over a wide range of temperatures. This behavior resembles the temperature dependence observed in Ar and Xe.<sup>2,3</sup> The electric field dependence of the electron drift velocity (or mobility) also behaves differently for these two classes of fluids with

branched alkanes and heavy Noble gases in one class and *n* alkanes and He, Ne in the other. It has been suggested that the excess electron might be in a delocalized state in the branched alkane fluids and in a localized state in the straight chain alkane fluids.

The energy of the bottom of the electron conduction band,  $V_0$ , determined by measuring the onset of electron photoconductivity from metal electrodes immersed in the fluid, mirrors the density dependence of the electron mobility in branched and straight chain alkane fluids.<sup>7</sup> It was found that  $V_0$  decreases, reaches a minimum at densities larger than the fluid critical density, and then increases as the density is increased to the dense fluid state regime. In branched alkane fluids, the minimum is at approximately the same density as the electron mobility maximum, while in the chain alkane fluids, the minimum is approximately at the density where the electron mobility shows a shoulder. The conduction band energy,  $V_0$ , has a relatively shallower minimum in chain alkanes than in the branched alkanes. (For example, the minimum of  $V_0$  in ethane,  $-0.18$  eV; propane,  $-0.27$  eV; butane,  $-0.18$  eV; normal pentane,  $-0.27$  eV; while in Methane,  $-0.39$  eV; neopentane,  $-0.52$  eV.)

Much theoretical work has been devoted to explaining the dichotomy between these two classes of solvents. The density dependence of  $V_0$  has been used to infer the energetically favorable excess electronic state in these fluids. Path integral Monte Carlo simulations of an excess electron in He and Xe have shown that the delocalization in Xe and localization in He are primarily due to distinct differences in electron molecule interaction potentials.<sup>8</sup> Because Xe has a large atomic polarizability, deep potential wells from different Xe atoms in fluids at high density create a network of connected channels of attractive potential energy through which the excess electron can ex-

tend and percolate. At low fluid densities, the attractive channels induce cluster formation and the excess electron gets self-trapped on the clusters. It was recently shown that many-body polarization interactions arising from induced-dipole-induced-dipole interactions are very important and must be included to account for the observed density dependence of the photoconductivity threshold,<sup>9</sup>  $V_0$ . In He, because of its very small atomic polarizability, the pseudopotential between the excess electron and the He atom is almost totally repulsive. The excess electron forms a cavity at high density by expelling the He around it, that is, the electron becomes self-trapped.

A RISM polaron approximation based on a pseudopotential in which the electron interacts with a fluid atom through a hard sphere potential has been used to model electron solvation in He and Xe by Laria and Chandler.<sup>10</sup> In He, the electron solvation was reproduced by choosing the hard core radius of the electron-He pseudopotential to be almost the same as the radius of the He-He interaction. In Xe, by assigning the electron-Xe pseudopotential a much smaller hard sphere radius than the hard sphere Xe-Xe interaction radius, Laria and Chandler were able to get agreement with Coker *et al.*'s path integral Monte Carlo simulations in high density Xe fluids. Because of the importance of the attractive interaction at low fluid densities, the behavior of the electron in Xe cannot be predicted with a hard sphere repulsive pseudopotential. Laria and Chandler concluded that the repulsive part of the potential, or the excluded volume, is the determining factor in electron solvation problems in He and high density Xe fluids, and that the excluded volume in Xe fluid is much smaller than the excluded volume in He at the same fluid density.

Can the simple RISM polaron model also explain the differences observed in alkane fluids? We have simulated a simple model suggested by the RISM polaron model in which the methyl and methylene groups are represented by soft spheres of diameter  $d$  for the repulsive cores seen by the electron, and diameter  $\sigma$  for repulsive cores seen by other methyl and methylene groups. We find that this simple model gives the same qualitative behavior for the excess electron in methane as in ethane (see Sec. IV C). It thus behooves us to explore electron-molecule pseudopotentials that are more general than simple electron-methylene site-site pseudopotentials.

A comparison of electron solvation in fluid ethane and methane should help us to understand how the presence of C-C bonds affects electron solvation. We have made an extensive study of an excess electron in fluid methane and ethane as a function of fluid density using a wide variety of theoretical methods. All alkane molecules have high polarizabilities. Nevertheless, electrons localize in high density ethane but not in high density methane (as in He vs Xe). Unlike the electron-He interaction, the electron-ethane interaction can be strongly attractive, so that the differences between electron solvation in fluid methane and ethane cannot be explained as simply as the differences between simpler solvents (such as Xe and He) by the presence of a network of attractive channels in the former, and the ab-

TABLE I. Pseudopotential parameters (in a.u.).

$A_1$	$B_1$	$A_2$	$B_2$
300.0	2.10	-132.0	1.87
$A_3$	$B_3$	$\alpha$	$r_0$
165.0	2.00	17.5	1.175

sence of those in the latter fluid. In addition, the differences between electron-molecule interaction pseudopotentials in methane and ethane are not as dramatic as in Xe and He fluids. For example, the dependence of  $V_0$  on density has a minimum in methane that differs from the minimum in ethane by only 0.2 eV,<sup>11,12</sup> whereas the density dependence of  $V_0$  in He is qualitatively different than in Xe.<sup>13,14</sup>

Central to the understanding of electron solvation is the correct description of the interaction potentials between the electron and the solvent. By analyzing electrical induction in the electron-methane and electron-ethane interaction, a simple pseudopotential model was developed for both the branched and chain alkane molecules. In this paper we focus on the simple case of electron solvation in methane and ethane fluids. We find that if a repulsive center is placed midway along the C-C bond in ethane, simulations give excellent agreement with experiment. This repulsive C-C bond site is expected from the electron density distribution determined from quantum chemical calculations as well as from considerations of electrical induction. This repulsive site C-C model not only gives excellent agreement with experiments on methane and ethane but, as will be shown in a subsequent publication, it also gives excellent agreement with experiment for neopentane and *n*-pentane.

In Sec. II we describe pseudopotentials. In Sec. III we describe the PIMC simulation method, the fast-Fourier-transform-Lanczos method, and the physical quantities used to characterize electron solvation properties. The results of extensive simulations are presented in Sec. IV.

## II. PSEUDOPOTENTIALS

Due to symmetry, methane does not have a permanent electrical dipole and quadrupole moment. Thus an electron interacting with an isolated methane molecule can be modeled by a spherical pseudopotential of the same form as used in our previous studies of an excess electron in Ar and Xe fluids:<sup>9</sup>

$$V(r) = A_1 e^{-B_1 r} + A_2 e^{-B_2 r} - \frac{\alpha e^2}{2r^4} S(r). \quad (2.1)$$

The first two exponential terms in Eq. (2.1) represent the repulsive pseudopotential arising from static and exchange interactions with the electron. The last term is the electron-induced dipole interaction potential. Here  $\alpha$  ( $= 17.5$  a.u.) is the gas phase polarizability of methane and  $S(r) = (1 - e^{-r/r_0})^6$  is the switching function for the polarization with  $r_0 = 1.175$  a.u. as used in *ab initio* calculations of electron-CH<sub>4</sub> elastic scattering.<sup>15</sup> The parameters in the repulsive terms (in Table I) were chosen to fit the electron

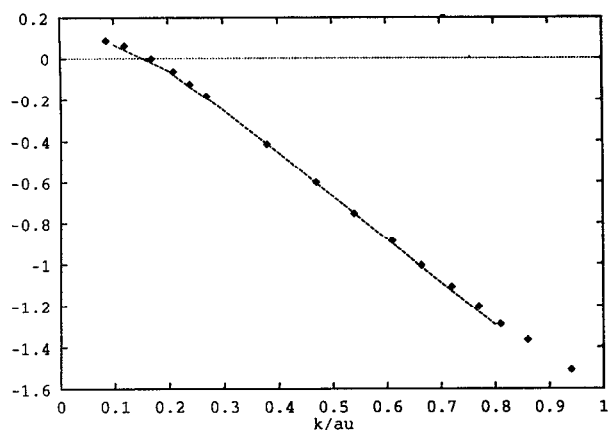


FIG. 1. Electron-methane  $S$ -wave phase shift  $\delta_0$  as a function of the initial electron kinetic energy. The diamonds are from a theoretical calculation by Yuan (Ref. 17) and the dashed line is the result calculated from our electron-methane pseudopotential.

$S$ -wave ( $l=0$ ) phase shift  $\delta_0$  data from *ab initio* calculations.<sup>16,17</sup> The phase shift  $\delta_0$  calculated from this pseudopotential agrees very well with the *ab initio* results as shown in Fig. 1. We obtained a scattering length of  $-2.4$  a.u., and found that the Ramsauer–Townsend effect, where  $\delta_0=0$ , occurs at  $0.35$  eV. These values compared well with the experimental values of  $-2.475$  a.u. and  $0.48$  eV, respectively. The pseudopotential given by Eq. (2.1), combined with the many-body polarization interactions between the induced dipoles (as discussed in Ref. 18) was used to calculate the excess electronic ground state energies,  $E_0$ , in fluid methane and gives good agreement with the experimentally measured  $V_0$  over a wide density regime.<sup>18</sup> The corresponding ground state wave functions, calculated using the Lanczos algorithm were found to be extended for all of the fluid densities studied.

The precise connection between the experimentally observed  $V_0$  values and the excess electron ground state energies,  $E_0$ , is nontrivial. As discussed in the introduction to the paper by Space *et al.*,<sup>9</sup> the density dependent  $V_0$  curve is bounded from below by the  $E_0$  curve. The reader should consult the discussion in this reference.

The electronic structure of the ethane molecule is such that there is a build up of electron density on the C–C bond. This negative charge gives rise to a strong repulsion of the excess electron near the C–C bond. The pseudopotential should therefore contain repulsive terms centered on the C atoms and on the center of the C–C bond. Also, the bond polarizability tensor corresponding to the C–C bond in ethane has two components,  $\alpha_{\parallel} = 12.7$  a.u. along the bond and  $\alpha_{\perp} = 0.1$  a.u. perpendicular to the bond.<sup>19</sup>  $\alpha_{\parallel}$  is almost as large as the polarizability of the methylene group itself, while  $\alpha_{\perp}$  is comparatively very small. Thus, because of this polarizability anisotropy, the induction energy of an excess electron will be much more attractive when the electron approaches the C–C bond along the direction parallel to the bond than when it approaches along the perpendicular direction. Furthermore, the

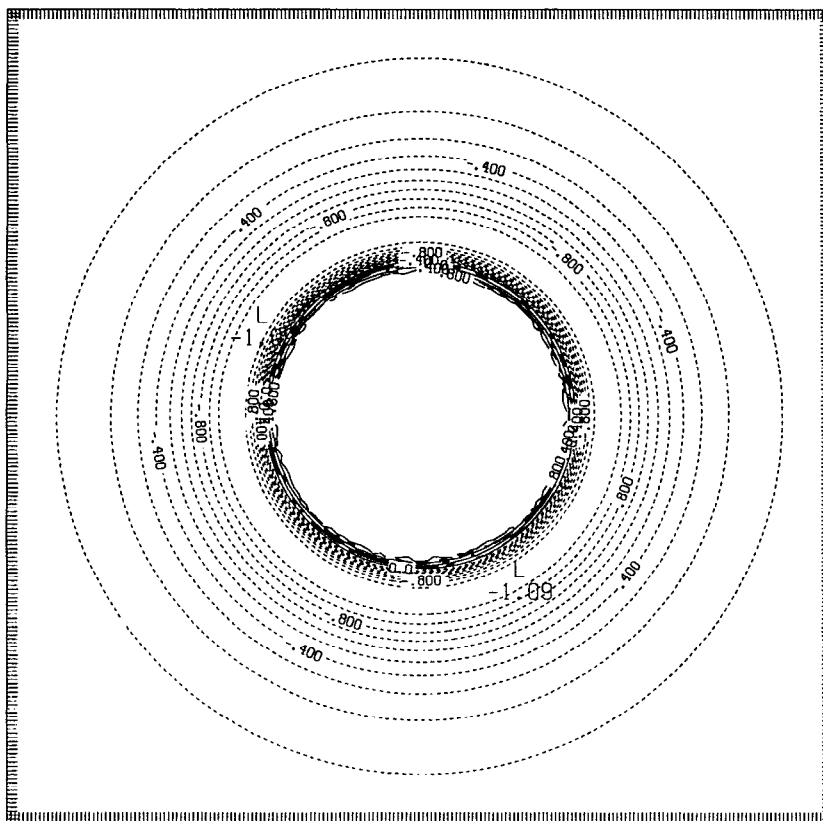
induced-dipole–induced-dipole interactions between the methyl groups, (with spherical polarizabilities) is much more repulsive when the electron approaches the ethane molecule along a direction perpendicular to the C–C bond than when it approaches along the parallel direction. Based upon the aforementioned analysis, we propose a simpler model which accounts for the asymmetric nature of the electron-ethane induction interaction by enhancing the physically necessary repulsive pseudopotential site at the center of the C–C bond. Our pseudopotential for the electron-ethane interaction is therefore a three site pairwise additive form,

$$V(r) = \sum_{i=1}^2 \left( A_1 e^{-B_1 r_i} + A_2 e^{-B_2 r_i} - \frac{\alpha e^2 S(r)}{2r_i^4} \right) + A_3 e^{-B_3 R}, \quad (2.2)$$

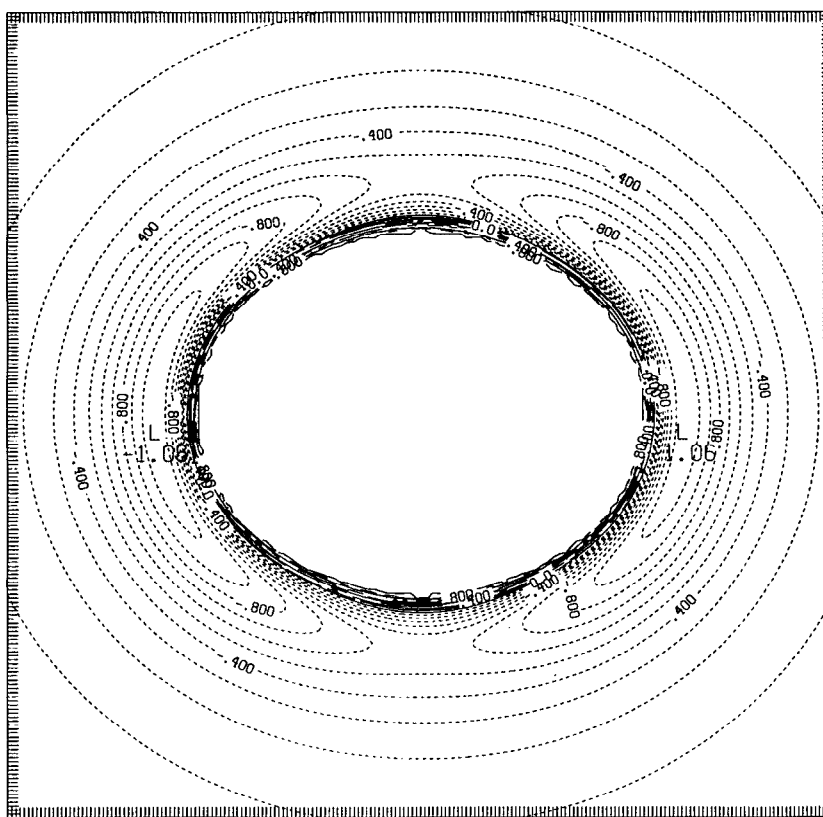
where the fourth term is therefore the aforementioned repulsive pseudopotential (assumed to be of the “Born–Mayer” type) between the electron and the center of the C–C bond at a distance of  $R$ . The parameters  $A_1$ ,  $A_2$ ,  $B_1$ ,  $B_2$ ,  $\alpha$ , and  $S(r)$  are taken to be the same as that in the electron-methane interaction. The parameters  $A_3=165.0$  and  $B_3=2.0$  were determined by using Eq. (2.2) to calculate the excess electron ground state energy in the unperturbed fluid ethane, propane, and *n*-pentane.<sup>18</sup> It is adjusted to give agreement with the experimental  $V_0$  for ethane as a function of density in the moderate density regime, as shown in Fig. 11. The calculations include the many-body polarization interaction between induced dipoles on different molecules, but because we have already approximated the intramolecular induced-dipole–induced-dipole interaction by placing an enhanced repulsive site on the C–C bond, we must avoid overcounting it. Thus we turn off the direct intramolecular dipole–dipole interactions.

We compare the full ethane model with a repulsive pseudopotential centered on the C–C bond to a model with this center omitted ( $A_3=0$ ). It will be seen that the model with  $A_3=0$  is completely inconsistent with experiment in that in both methane and ethane the electron is in an extended state for the full density regime studied. It is also of considerable interest to compare the predictions of the full model to that of the simple RISM polaron model. We have explored a simple model in which the methyl and methylene groups are represented by spheres of diameter  $d$  for the repulsive cores seen by the electron and diameter  $\sigma$  for repulsive cores seen by other methyl and methylene groups. It will be seen that this RISM polaron model also predicts similar excess electron properties for both methane and ethane.

Contour plots of the electron-molecule interaction pseudopotential models for methane [Eq. (2.1)] and ethane [Eq. (2.2)] are shown in Fig. 2. As expected, the short-range electron-ethane pseudopotential is nonspherical with a pseudopotential minimum at each end of the molecule and a belt of saddle points around the middle of the C–C bond. It can be seen that the well depth of the electron-ethane pseudopotential is as deep as in electron methane.



(a) CONTOUR FROM -1.0000 TO 1.0000 CONTOUR INTERVAL OF 0.10000 PT(3,31) = -0.15757E-01



(b) CONTOUR FROM -1.0000 TO 1.0000 CONTOUR INTERVAL OF 0.10000 PT(3,31) = -0.33647E-01

FIG. 2. Contour plots of the electron-molecule pseudopotential in eV. (a) The electron-methane potential contour. (b) The  $e^-$ -ethane cross section potential contour.

Alkanes are highly polarizable molecules. The polarizability of methane (or the methyl group) is comparable to the polarizability of Kr ( $\alpha_{\text{Kr}}=16.6$  a.u.). Because these polarizabilities are so large, when an electron interacts with one or more alkane molecules the induced dipole-dipole interaction makes a large contribution to the energetics of the solvated electron.<sup>5,9</sup> This many-body polarization effect is described by a self-consistent set of field equations, which in the dipole-dipole approximation, take the form

$$\mathbf{E}_i = \mathbf{E}_i^0 + \alpha \cdot \mathbf{T}_{ij} \cdot \mathbf{E}_j, \quad (2.3)$$

with the corresponding polarization energy given by

$$V_p(r) = -\frac{1}{2} \alpha \sum_i \mathbf{E}_i^0 \cdot \mathbf{E}_i. \quad (2.4)$$

In Eqs. (2.3) and (2.4)  $\mathbf{E}_i^0$  is the bare (unscreened) field from the electron and  $\mathbf{E}_i$  is the local field at the site  $i$  in the fluid. As has already been pointed out, the intramolecular dipole-dipole interaction between methyl-methyl sites is ignored because it is accounted for by the placement of an enhanced repulsive site on the C-C bond. Thus, in Eq. (2.3), the dipole propagator connecting two methyl sites on the same molecule is taken to be zero.

The field equations can be solved by matrix inversion for each configuration of the solvent as has been done in our previous studies of electron solvation in fluids like water, Xe and Ar, and in small clusters of simple inert gas molecules.<sup>9,20</sup> For large systems, however, direct inversion of the matrix for each fluid configuration requires intensive computation and becomes practically infeasible. A good approximation is to multiply the polarizability  $\alpha$  by the Lorentz factor  $f_L = 1/(1 + 8\pi\rho\alpha/3)$ , where  $\rho$  is the density of the solvent atoms which has a polarizability of  $\alpha$ . This approximation only reduces the polarizability of the molecules by a density dependent screening factor and thus the electron-solvent interaction pseudopotential is still pairwise additive. Although this approximation might appear to be very crude, the important density dependence of the polarization interactions between the electron and solvent has been implicitly included without increasing the computational effort. The main contribution to the total potential energy of the solvated electron is from atoms at large distances so that it is customary to treat this distant part of the solvent as a continuum in the simulations. Even for atomic sites close to the electron, the approximation is only slightly less attractive than predicted by the full many-body calculation. It has been shown for electron solvation in Xe that the approximation using the Lorentz factor  $f_L$  predicts potential energies only 10% larger than the full many-body calculation.<sup>5</sup> This treatment is a mean-field treatment of the long-range interaction in isotropic fluids. It will break down in systems containing large molecules and in ordered systems like liquid crystals and solids.

In this paper, the methyl groups are approximated as extended atoms and methyl groups on different ethane molecules interact through a site-site Lennard-Jones potential with the same parameters as used in the methane-methane interactions. Thus

$$V_{S-S}(r) = 4\epsilon[(\sigma/r)^{12} - (\sigma/r)^6], \quad (2.5)$$

where  $\sigma = 3.923 \text{ \AA}$  and  $\epsilon/k_B = 72 \text{ K}$ ,  $k_B$  is the Boltzmann constant, and the C-C bond in ethane is taken as rigid with a bond length of  $1.53 \text{ \AA}$ .

### III. METHODOLOGY

#### A. Path integral staging Monte Carlo

As usual, the partition function can be expressed as the trace over the density matrix. In the position representation,

$$Z(\beta) = \int d\mathbf{r} \rho(\mathbf{r}, \mathbf{r}, \beta) = \int d\mathbf{r}_1, \dots, d\mathbf{r}_p \prod_{i=1}^p \rho(\mathbf{r}_i, \mathbf{r}_{i+1}, \tau), \quad (3.1)$$

where  $\beta = 1/k_B T$ ,  $\mathbf{r}_1 = \mathbf{r}_{p+1} = \mathbf{r}$ , and the imaginary (or Euclidean) time is  $\tau = \beta/P$ .<sup>21</sup>

The density matrix at high temperature, or concomitantly, at short time  $\tau = \beta/P$ , can be expressed as the primitive short time (high temperature) approximation:

$$\begin{aligned} \rho(\mathbf{r}_i, \mathbf{r}_{i+1}; \tau) &= \exp\left(-\frac{\tau V(\mathbf{r}_i)}{2}\right) \rho_0(\mathbf{r}_i, \mathbf{r}_{i+1}; \tau) \\ &\quad \times \exp\left(-\frac{\tau V(\mathbf{r}_{i+1})}{2}\right) + O[\tau^3], \end{aligned} \quad (3.2)$$

where

$$\rho_0(\mathbf{r}_i, \mathbf{r}_{i+1}; \tau) = \left(\frac{m}{2\pi\hbar^2\tau}\right)^{3/2} \exp\left(-\frac{m}{2\hbar^2\tau} (\mathbf{r}_i - \mathbf{r}_{i+1})^2\right) \quad (3.3)$$

is the free particle density matrix.

For an excess electron in a fluid, the system Hamiltonian is

$$H = -\frac{\hbar^2}{2m_e} \nabla^2 - \frac{\hbar^2}{2M_S} \sum_{i=1}^N \nabla_i^2 + U_{e-S} + U_{S-S}, \quad (3.4)$$

where  $M_S$  is the mass of the solvent atom and  $m_e$  is the mass of the excess electron. The electron-solvent atom and solvent atom-solvent atom interaction potentials are not generally pairwise additive, but if we adapt the self-consistent screening function in the Lorentz approximation, the final result becomes pairwise additive:

$$U_{e-S} = \sum_{i=1}^N V_{e-S}(|\mathbf{r}_i - \mathbf{R}_i|), \quad (3.5)$$

$$U_{S-S} = \sum_{i=1}^{N-1} \sum_{j=i+1}^N V_{S-S}(|\mathbf{R}_i - \mathbf{R}_j|). \quad (3.6)$$

Since the solvent atom in our system is much heavier than the electron, the thermal wavelength for the solvent atom at the simulation temperature  $\lambda_s = \beta\hbar^2/M_S$  is much smaller

than the electron thermal wavelength  $\lambda_e$ . The density matrix for the solvent atom can be approximated by

$$\rho_0^s(\mathbf{R}_i, \mathbf{R}_{i+1}, \tau) = \delta(\mathbf{R}_i - \mathbf{R}_{i+1}). \quad (3.7)$$

Then the partition function of our system in the discretized path integral form is

$$\begin{aligned} Z_P(\beta) = & \left( \frac{m_e}{2\pi\hbar^2\tau} \right)^{3P/2} \int d\mathbf{R} e^{-\beta U_{S-S}(\mathbf{R})} \int dr_1 \cdots \int dr_P \\ & \times \exp \left[ -\beta \sum_{i=1}^P \left( \frac{m_e P}{2\hbar^2\beta^2} (r_i - r_{i+1})^2 \right. \right. \\ & \left. \left. + \frac{1}{P} U_{e-S}(r_i, \mathbf{R}) \right) \right]. \end{aligned} \quad (3.8)$$

This is the Born–Oppenheimer approximation in the path integral representation where the solvent atoms are taken as classical particles. The excess electron becomes an isomorphic classical cyclic chain polymer consisting of  $P$  particles (beads) interacting with the classical solvent atoms with an attenuated potential  $U_{e-S}/P$ , and connected with their nearest neighbors through a harmonic potential of force constant  $m_e P / (\beta\hbar)^2$ . As  $P \rightarrow \infty$  the approximate partition function  $Z_P(\beta) \rightarrow Z(\beta)$  and for finite  $P$ ,  $Z_P(\beta) \geq Z(\beta)$ . This quantum-classical isomorphism is thus a good approximation only if the number of beads  $P$  is large enough so that the rms bond length of the free classical chain,  $\sqrt{3}\lambda_e/\sqrt{P}$ , is small compared to the length scale over which the pseudopotential energy surface changes. Thus the convergence with  $P$  depends on the details of the interaction pseudopotential as well as on the temperature. If a large  $P$  is required, as is often in the case for electron solvation problems, the harmonic potential between neighboring beads becomes stiff and the primitive path integral Monte Carlo method becomes very inefficient. An efficient Staging Monte Carlo algorithm<sup>22,8,20</sup> which samples the harmonic interaction directly and makes a displacement for many beads simultaneously can be used to insure rapid convergence.

The physical size of the electron chain can be characterized by the mean square displacement between pairs of beads on the chain separated by different imaginary time increments  $\tau = t - t'$ ,

$$\mathcal{R}^2(t-t') = \langle |\mathbf{r}(t) - \mathbf{r}(t')|^2 \rangle, \quad (3.9)$$

where  $0 < t - t' \leq \beta\hbar$ . For a free particle, this correlation function is parabolic

$$\mathcal{R}_{\text{free}}^2(t-t') = 3\lambda_e^2(t-t')(\beta\hbar - t + t') / (\beta\hbar)^2 \quad (3.10)$$

with maximum value at  $\beta\hbar/2$ . For the free particle,  $\mathcal{R}_{\text{free}}^2(\beta\hbar/2) = 3\lambda_e^2/4$ . This function has been used as a signature of electron localization.<sup>23,8</sup> For a localized electron with ground state dominance, this curve deviates from the free electron parabolic curve and becomes independent of  $\tau$  except near 0 and  $\beta\hbar$ . For delocalized electron,  $\mathcal{R}^2(t-t')$  is close to the free particle curve and is parabolic at all  $\tau$ .

We define the probability distribution functions

$$S_{b-\text{com}}(r) = \left\langle \sum_{i=1}^P \delta(\mathbf{r}_i - \mathbf{r}_{\text{com}} - \mathbf{r}) \right\rangle \quad (3.11)$$

and

$$g_{c-\text{com}}(r) = \rho^{-1} \left\langle \sum_{i=1}^N \delta(\mathbf{R}_i - \mathbf{r}_{\text{com}} - \mathbf{r}) \right\rangle, \quad (3.12)$$

where  $\rho$  is the solvent number density,  $S_{b-\text{com}}(r)$  is the normalized probability distribution function of the relative position of the electron beads with respect to the center of mass (com) position  $\mathbf{r}_{\text{com}} = \sum_{i=1}^P \mathbf{r}_i / P$ , or centroid of the cyclic polymer chain representing the quantum electron and  $g_{c-\text{com}}(r)$  is the pair correlation function of a fluid atom with respect to the barycenter of the isomorphic electron.

It is easy to show that for a free excess electron at temperature  $T$ ,

$$S_{b-\text{com}}^{\text{free}}(r) = (2\pi w^2)^{-3/2} e^{-r^2/2w^2}, \quad (3.13)$$

where  $w^2 = \lambda_e^2(1 - 1/P^2)/12$  is a function of the number of beads  $P$ .

In simulations it is useful to compare  $S_{b-\text{com}}(r)$  and  $g_{c-\text{com}}(r)$  for the same fluid and chain configurations. For a free electron,  $g_{c-\text{com}}(r) = 1$  for all  $r$  since the electron does not feel the solvent atoms. If the electron forms a well defined cavity in the solvent,  $g_{c-\text{com}}(r) = 0$  within a certain small radius depending on the size of the cavity. These two quantities were used to characterize the spatial extent of the electron wavefunction and the solvent atom distribution around the electron.

The electron bead-solvent atom pair distribution function provides information about the local fluid structure around the electron beads

$$g_{e-c}(r) = \rho^{-1} \left\langle \sum_{i=1}^N \frac{1}{P} \sum_{k=1}^P \delta(\mathbf{R}_i - \mathbf{r}_k - \mathbf{r}) \right\rangle. \quad (3.14)$$

## B. FFT-Lanczos algorithm

The FFT-Lanczos diagonalization algorithm calculates instantaneous adiabatic electronic eigenvalues and eigenfunctions on a discrete grid of  $M$  points in the configuration space by using an efficient scheme based on an iterative Lanczos method.<sup>24,25,9</sup> In this discretized space representation, the Hamiltonian  $H$  is a  $M \times M$  matrix in the configuration representation whose low energy eigenstates are to be determined. The eigenstates of  $\exp(-\tau H)$  are the same as those of  $H$  but the iterative Lanczos method converges faster for a large enough value of  $\tau$ .<sup>25</sup> The short time approximation of the propagator  $\exp(-\tau H)$ , based on the reversible Trotter factorization,

$$\exp(-\tau H) = \exp\left(-\frac{\tau T}{2}\right) \exp(-\tau V) \exp\left(-\frac{\tau T}{2}\right) + O(\tau^3) \quad (3.15)$$

(where  $T$  and  $V$  are the kinetic and potential operators of the excess electron), was used, in conjunction with standard fast Fourier transform methods, to compute the ac-

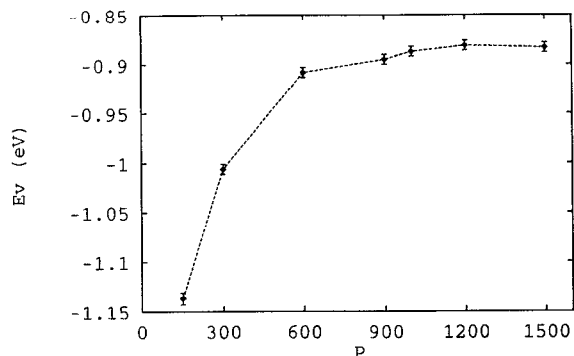


FIG. 3. The electronic potential energy as a function of the number of discretization points,  $P$ , in the electron path integral. The electron-ethane system is simulated at  $T=340$  K and  $\rho^*=0.5$ .

tion of this short time propagator on an arbitrary initial wave function. The Lanczos recursion was implemented to find the largest eigenvalues of this short time approximation. The electronic ground state energy was calculated accurately with an annealing sequence using the single vector Lanczos algorithm by starting with a large  $\tau$  to determine an approximate ground state eigenfunction. With this as the starting state the procedure is repeated for smaller  $\tau$ 's until convergence is obtained.

The FFT-Lanczos was used to calculate the electronic energies and their corresponding wave functions in frozen solvent configurations. The electron equilibrated solvent configuration was generated by the PIMC simulation. The neat solvent configuration was generated at the same thermodynamic conditions as in the PIMC but without the electron. The effect of the electron on the solvent was probed by comparing the electronic properties in unperturbed and relaxed fluids.

#### IV. RESULTS

Electron solvation in methane was studied by simulating an electron in a primary cubic cell of length  $L$  containing  $N$  methane molecules under periodic boundary conditions. The methane molecules are treated as Lennard-Jones spheres of diameter  $\sigma$  and with well depth  $\epsilon$ . The reduced critical density and temperature for a monoatomic Lennard-Jones fluid is  $\rho_c^* = \rho_c \sigma^3 = 0.33$  and  $T_c^* = kT/\epsilon = 1.30$  translates into critical parameters  $\rho_c = 5.5 \times 10^{21} \text{ cm}^{-3}$  and  $T_c = 94$  K for methane. The simulations reported below were done at the supercritical temperature

TABLE II. Convergence of ground state energies (in eV) with the number of spatial grid points  $M$  ( $\tau=0.1$ ).

$\rho^*$	Grid size ( $M^3$ )		
	$16^3$	$32^3$	$64^3$
	Methane		
0.5	-0.458	-0.318	-0.310
	Ethane		
0.6	0.124	0.158	0.168

TABLE III. Convergence of ground state energies (in eV) with  $\tau$  ( $M=32$ ).

$\rho^*$	$\tau$			
	0.3	0.2	0.1	0.05
	Methane			
0.5	-0.330	-0.319	-0.318	-0.318
	Ethane			
0.1	-0.0627	-0.0615	-0.0606	-0.0603
0.6	0.133	0.150	0.158	0.161

of  $T=340$  K ( $3.6T_c$ ). At this temperature, the thermal de Broglie wavelength of the excess electron is  $\lambda_e = (\beta \hbar^2 / m_e)^{1/2} = 16.125 \text{ \AA}$ . To avoid large perturbations of the excess electron we always take  $L$  to be larger than  $2\lambda_e$ . Because the properties of the electron are studied as a function of fluid density, the number of molecules in the primary box,  $N = \rho L^3$ , will be different for different densities.

As mentioned in Sec. III A, the classical isomorphism is accurate only for sufficiently large values of  $P$ . The convergence of the PIMC simulation as a function of  $P$  was tested at  $T=340$  K and  $\rho^*=0.5$  for ethane. Figure 3 shows that the electronic potential energy becomes independent of  $P$  for  $P > 900$  giving convergence within small error bars. From molecular symmetry it is reasonable to believe that the potential energy surface in methane is at least as smooth as that in ethane. Thus, in all of our simulations at 340 K, we used  $P=1000$ . The convergence of the FFT-Lanczos calculation as a function of the number of spatial grid points,  $M$ , is presented in Table II. The electronic ground state energies are calculated for high density methane and ethane. The results are well converged at  $M=32$  for both fluids. Table III presents the dependence of the electronic ground state energy on  $\tau$  in both methane and ethane fluids. The calculated energies

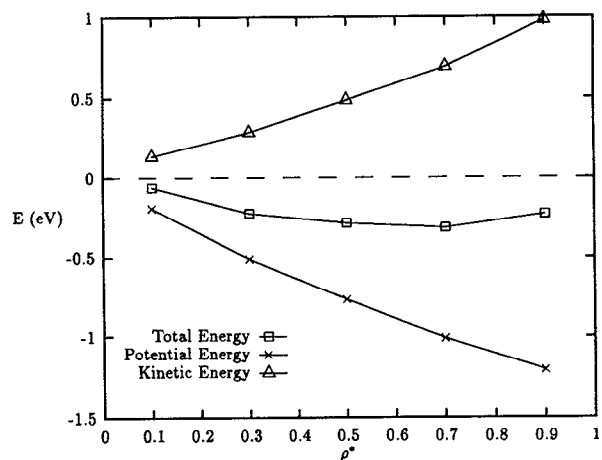


FIG. 4. The potential (cross), kinetic (square), and total (diamond) energy of the solvated excess electron in methane as functions of methane density at  $T=340$  K. The total energy has a minimum at about  $\rho^*=0.7$ .

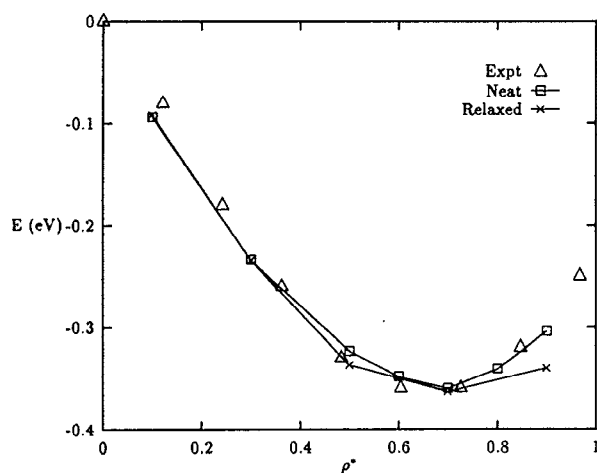


FIG. 5. The electronic ground state energy in electron equilibrated (cross) and neat (square) methane as a function of density. The triangle points are experimental  $V_0$  values measured by Asaf *et al.* (Ref. 11).

are well converged at  $\tau=0.1$ . We used  $M=32$  and  $\tau=0.1$  for all of our subsequent FFT-Lanczos calculations reported later.

All the interactions in these simulations were truncated at  $2.5\sigma$  but because the electron-induced dipole interactions are long ranged it is necessary to correct this by assuming a continuous distribution beyond the potential cutoff distance and integrating the potential function from the cutoff distance to infinity. The electronic kinetic energy was calculated from both the primitive kinetic energy estimator and the virial estimator with periodic boundary conditions.<sup>8</sup>

For all the PIMC simulation results reported here, the solvent molecules are initially placed on a fcc lattice. The initial positions of the electron polymer beads were sampled randomly within a sphere of radius  $\lambda_e/2$  situated at the center of the primary cell. Any electron bead-solvent atom overlaps (which give positive potential energies) were avoided by resampling the electron position. Moves of the electron beads were generated using the Staging algorithm and the attempted moves of the solvent atoms were separately accepted with the Metropolis criterion. The Monte Carlo acceptance ratios for both of the above moves are approximately 0.4. The initial configurations were annealed until the potential energies stabilized (typically within 3000 passes), then averages were accumulated for the next 10 000 passes. As usual, in one Monte Carlo (MC) pass, all of the beads in the polymer chain and all of the solvent atoms make one attempted move each.

### A. Methane

The electron-methane interaction in our model is spherically symmetric with an attractive pseudopotential well depth of approximately about 1.1 eV. The potential energy equals zero at  $0.406\sigma$  which makes the repulsive radius for the excess electron smaller than the Lennard-Jones (LJ) intermolecular repulsive radius ( $0.5\sigma$ ). At liquid densities the potential wells from nearest neighbor

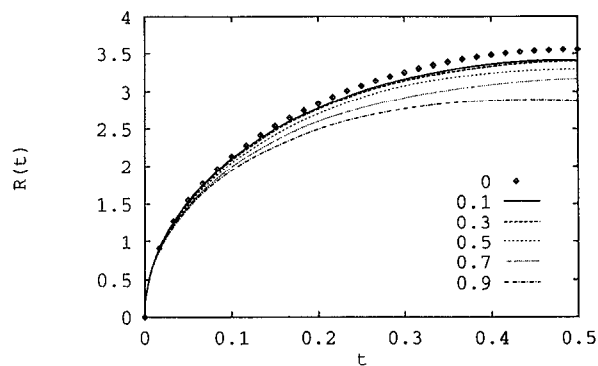


FIG. 6. The imaginary time correlation function,  $R(\tau)$  [cf. Eq. (3.9)], for the electron beads at various densities of methane at  $T=340$  K.

methane molecules overlap with each other and form deep channels extending through the whole simulation cell as in the case of Xe fluid. Like the PIMC simulation of Xe,<sup>5</sup> with a mean-field screening function, our electron-solvent interaction potential is explicitly solvent density dependent. As we already know from the Xe simulations, this density dependent potential produces qualitatively correct solvation energies as opposed to what would be predicted on the basis of a pair potential theory (which severely overestimates the attractive solvation energy).

Figure 4 displays the density dependence of the average electronic energy of the solvated electron calculated from the PIMC simulations. As the methane density increases, the total electronic energy decreases monotonically to a minimum around  $\rho^*=0.7$  and then starts increasing. This behavior coincides with the density dependence of the experimentally measured threshold for photoconductivity,  $V_0$ . The break up of the total energy into potential and kinetic components is also presented in Fig. 4. Both the electronic potential and kinetic energy change monotonically with increasing fluid density, but the potential energy levels off while the kinetic energy increases at a faster rate at high densities. This behavior in methane is very similar to the results found in simulations

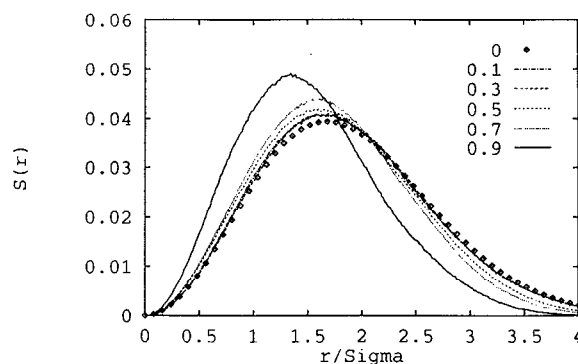


FIG. 7. The radial distribution function of the electron beads around their com,  $S_{b-com}$ , in methane at the reduced fluid densities 0.1, 0.3, 0.5, 0.7, and 0.9. The diamond points are the distribution function for the free electron calculated analytically with  $P=1000$ .

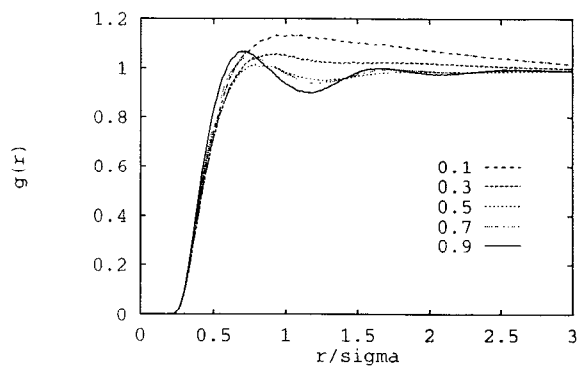


FIG. 8. The electron-solvent pair correlation function  $g_{e-c}(r)$  for the indicated densities of methane at  $T=340$  K.

of electron solvation in fluid Xe,<sup>5</sup> where many-body polarizations have been treated. As pointed out in a previous paper,<sup>9</sup> many-body polarization interactions increase the repulsive core of the potential and decrease the depth of the attractive well at high solvent densities. Since the kinetic energy is sensitive to the radius of the repulsive core which defines the "free volume" available to the solvated electron, the electronic kinetic energy more quickly increases with density because of the many-body polarization interactions and therefore is responsible for the position of the minimum in the total energy. The effect of the many-body polarization not only changes the behavior of the electronic energy, it also affects other solvation properties of the electron and the solvent structures as presented below.

In general, the presence of an excess electron will change the structure of a solvent in order to minimize the

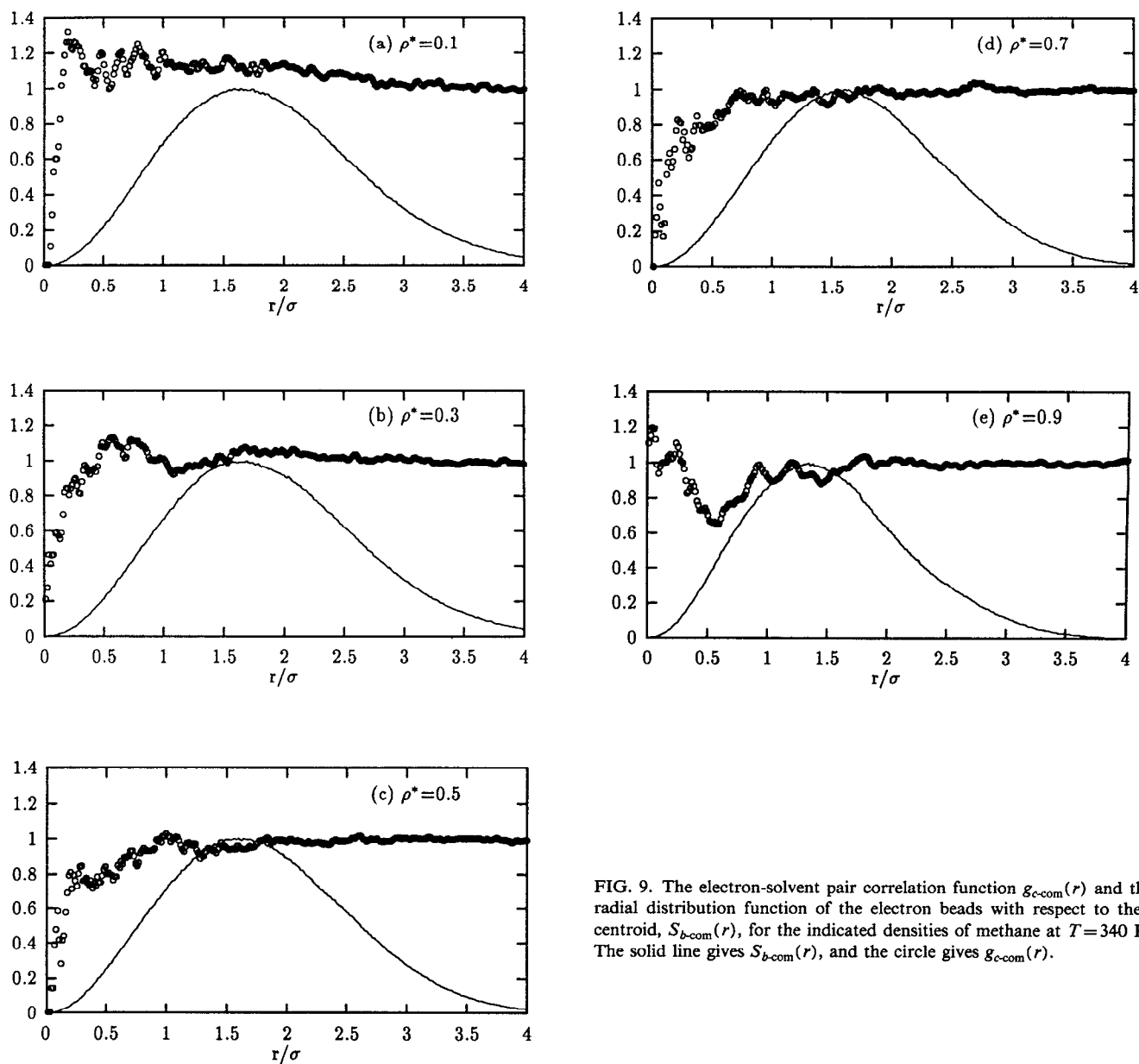


FIG. 9. The electron-solvent pair correlation function  $g_{e-com}(r)$  and the radial distribution function of the electron beads with respect to their centroid,  $S_{b-com}(r)$ , for the indicated densities of methane at  $T=340$  K. The solid line gives  $S_{b-com}(r)$ , and the circle gives  $g_{e-com}(r)$ .

free energy of the solution. This is most pronounced in solvents in which the electron becomes self-trapped in a cavity. Then solvent atoms are excluded from the cavity. In contrast, in high-mobility fluids the electron will be found in an extended state and the solvent structure will not be strongly perturbed. To study the reorganization of the solvent around the electron we have performed two different simulations. At a given solvent density and temperature we first equilibrate the neat solvent. FFT-Lanczos calculations are made of the electronic energies and wave functions of an excess electron inserted into typical frozen configurations of the neat solvent. At the same solvent density and temperature, PIMC simulations of the excess electron and solvent give configurations of the relaxed solution. FFT-Lanczos calculations of an excess electron in the typical relaxed fluid configurations give electronic energies and wave functions for the relaxed fluids. The results for the ground state energy of the excess electron in methane are displayed in Fig. 5. It can be seen that there are very small energy differences between the neat and electron relaxed configurations from  $\rho^* = 0.1$  to 0.7. At  $\rho^* = 0.9$  the electron has a lower ground state energy (about 0.05 eV) in the relaxed fluids than in the neat solvent. This behavior is typical of an extended electron. The electron-Xe system<sup>26</sup> behaves almost identically to Fig. 5.

Figure 6 gives the density dependence of the imaginary time correlation function,  $\mathcal{R}(\tau)$  [cf. Eq. (3.9)], of the electron in methane. The correlation function is weakly dependent on the fluid density. Over all densities from  $\rho^* = 0.1$  to  $\rho^* = 0.7$ ,  $\mathcal{R}(\tau)$  lies very close to the free particle parabola and behaves like that of a quasifree electron. At density  $\rho^* = 0.9$ ,  $\mathcal{R}(\tau)$  deviates from the free particle curve and reaches approximately 80% of the free particle value at  $\tau = 0.5$ . The curve begins to flatten near  $\tau = 0.5$ , indicating that the electron may be starting to show a hint of ground state dominance and become slightly trapped at  $\rho^* = 0.9$ . However, it does not show the strong character of localization. The distribution function of the electron beads around their com,  $S_{b\text{-com}}(r)$ , for different densities is given in Fig. 7. These curves are very close to the free particle curve up to  $\rho^* = 0.7$ . At  $\rho^* = 0.9$ , the peak of the curve has a displacement toward small  $r$  and the width of the peak is less than the free particle width. This shows that the distribution of electron beads has been compressed by the solvent at  $\rho^* = 0.9$ .

The electron-methane radial distribution function,  $g_{e-c}(r)$ , is presented as a function of density in Fig. 8. The distance of closest approach of the electron to the carbon atom is about 0.78 Å ( $0.2\sigma$ ) and is independent of the fluid density. This is due to tunneling of the electron into the repulsive region of the potential. There is a nonmonotonic density dependence of the initial rise in  $g_{e-c}(r)$  due to the many-body polarization interaction. Nonmonotonicity also appears in electron solvation in He and hard-sphere solvents<sup>8,23</sup> but not for the same reason. At  $\rho^* = 0.1$ , the first peak of  $g_{e-c}(r)$  is larger than unity and extends to  $2.5\sigma$  suggesting that the excess electron is located on a cluster of solvent molecules with reduced density higher than 0.1. The pair correlation function  $g_{e-c}(r)$  starts to show struc-

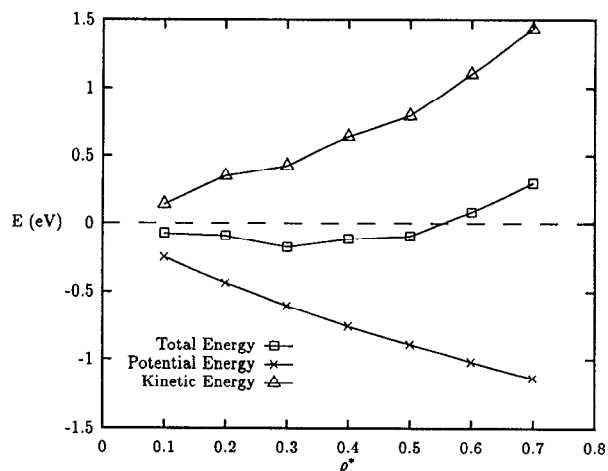


FIG. 10. The potential (cross), kinetic (square), and total (diamond) energies of the solvated excess electron in ethane as functions of ethane density at  $T = 340$  K. The total energy has a minimum at about  $\rho^* = 0.3$  and becomes positive at densities higher than  $\rho^* = 0.5$ .

ture above  $\rho^* = 0.5$ . The first and second nearest neighbor peaks appears at density  $\rho^* = 0.7$  and 0.9, respectively, and are located at approximately  $0.5\sigma$  and  $1.5\sigma$ , respectively, suggesting that the electron polymer is in an extended state (or delocalized) at these densities. If the electrons were localized in a cavity of radius  $a$ , this radial distribution function would not exhibit well defined peaks because beads in the center of the cavity and beads near the surface of the cavity are at different distances from the first and second nearest neighboring solvent atoms; thus averaging over all of the bead positions will wipe out the structure.

The methane radial distribution function  $g_{c\text{-com}}(r)$  and the electron beads radial distribution function  $S_{b\text{-com}}(r)$  are displayed in the same plot in Fig. 9 at all the solvent densities. Here the  $S_{b\text{-com}}(r)$  are normalized such that the amplitude of the peak is unity. The relative area under  $S_{b\text{-com}}(r)$  from 0 to  $r$  gives the the fraction of electron beads within  $r$  and therefore the probability of finding the electron inside a sphere of radius  $r$  with respect to the electron com. For all the methane fluid densities from  $\rho^* = 0.1$  to 0.9, the electron beads extend from their com to a distance larger than  $2.5\sigma$  into the solvent. The distribution of the solvent atoms around the barycenter of the electron beads is almost uniform, which indicates that there is no cavity formation around the electron. At very small distances the small number of data counts give rise to large relative errors in  $g_{c\text{-com}}(r)$ .

In summary, for methane, the excess electron is found in an extended state for all the densities studied. At  $\rho^* = 0.1$ , the local solvent around the electron has a higher density than 0.1, and there is electron induced cluster formation. At  $\rho^* = 0.9$ , the local solvent around the electron has a lower density than 0.9 and the electron stays in this dilute region. At the intermediate densities, the excess electron does not change the local solvent density and does not become self-trapped.

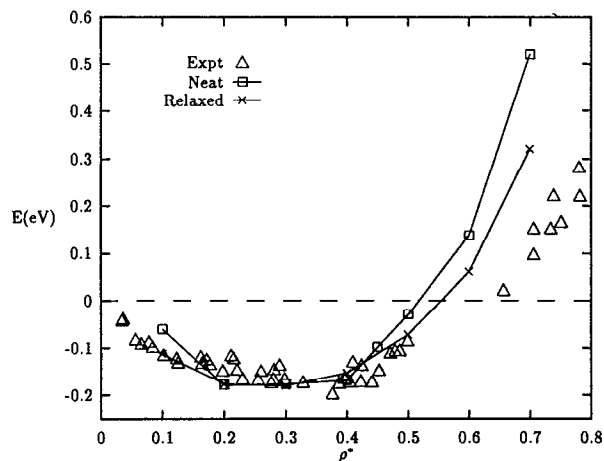


FIG. 11. The electronic ground state energy as a function of density in electron equilibrated (cross) and neat (square) ethane fluid. The triangle points are experimental  $V_0$  values measured by Yamaguchi *et al.*<sup>12</sup>

### B. Ethane: Three-site model

Ethane was simulated for the density regime  $0.1 \leq \rho^* = \rho\sigma^3 \leq 0.7$ , where  $\rho$  is the number density of ethane molecules and  $\sigma$  is the LJ diameter of the methyl groups. This density regime covers the entire range of ethane fluid densities studied by experiment. The shoulder of the mobility curve and the minimum of  $V_0$  are at densities between  $\rho^* = 0.3$  and  $\rho^* = 0.4$ . For densities larger than  $\rho^* = 0.4$ , the electronic mobility decreases monotonically with increasing ethane density. The electron-ethane pseudopotential is asymmetric. When the electron approaches ethane parallel to the C-C bond, the electron-carbon atom potential energy vanishes at  $r = 0.41\sigma$ , a distance smaller than the LJ intermolecular repulsive radius for  $\text{CH}_3$  ( $0.5\sigma$ ) and thus gives a positive skin thickness. When the electron approaches ethane along a direction perpendicular to the C-C bond, the electron-carbon atom potential energy vanishes at  $r = 0.56\sigma$ , a distance larger than the LJ intermolecular repulsive radius of  $\text{CH}_3$  and

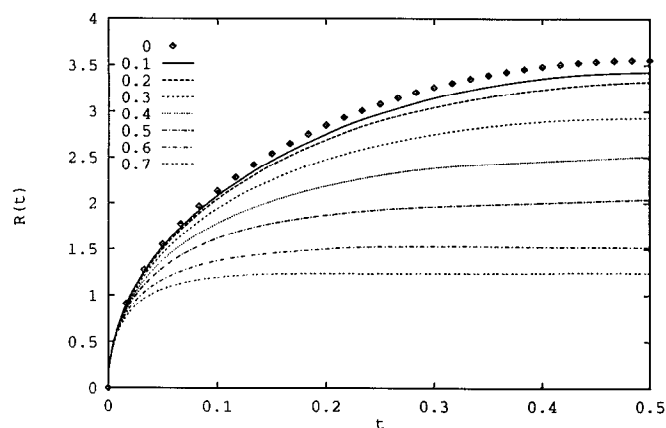


FIG. 12. The imaginary time correlation function,  $R(\tau)$  [cf. Eq. (3.9)], at the indicated ethane densities at  $T = 340$ .

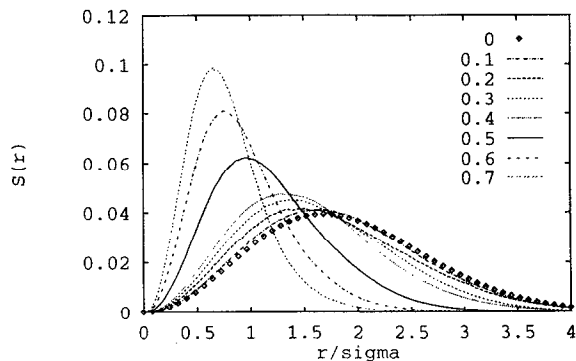


FIG. 13. The radial distribution function of the electron beads around their barycenter,  $S_{b,\text{com}}(r)$ , in ethane the indicated ethane densities. The diamond points are the distribution function for the free electron.

thus gives rise to a repulsive bulge. At liquid densities, depending on the packing of the ethane molecules, some configurations in the liquid will provide deep attractive potential channels to the electron, but other configurations of attractive channels will terminate in repulsive walls. Unlike the electron solvation in methane, contiguous attractive potential channels will cease to exist and thus paths associated with an extended electron will be eliminated in ethane.

The bond length of the ethane molecules is kept constant in our simulations. In ethane, the Metropolis MC method was implemented by moving the center of mass and rotating the molecule around one of the three space-fixed axes (through the center of mass) chosen at random.<sup>27</sup>

Figure 10 displays the density dependence of the average electronic energies of the solvated electron from the PIMC simulation. As the solvent density increases, the total energy decreases monotonically to a minimum of  $-0.178$  eV at  $\rho^* = 0.3$ , and then starts rising and becomes positive after  $\rho^* = 0.5$ . This behavior coincides with the density dependence of the experimentally measured  $V_0$ . The break up of the total energy into potential and kinetic components is also displayed in Fig. 10. Both the electronic potential and kinetic energy change monotonically with

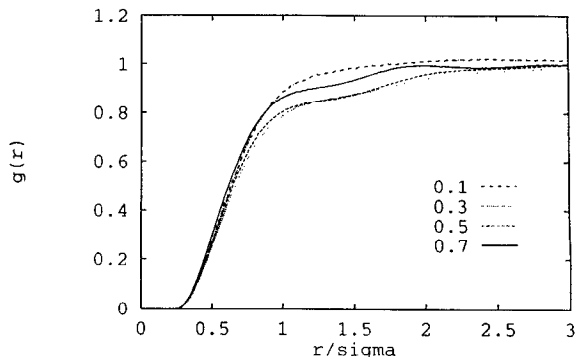


FIG. 14. The electron-carbon radial distribution function  $g_{e-c}(r)$  for the indicated densities of ethane at  $T = 340$  K.

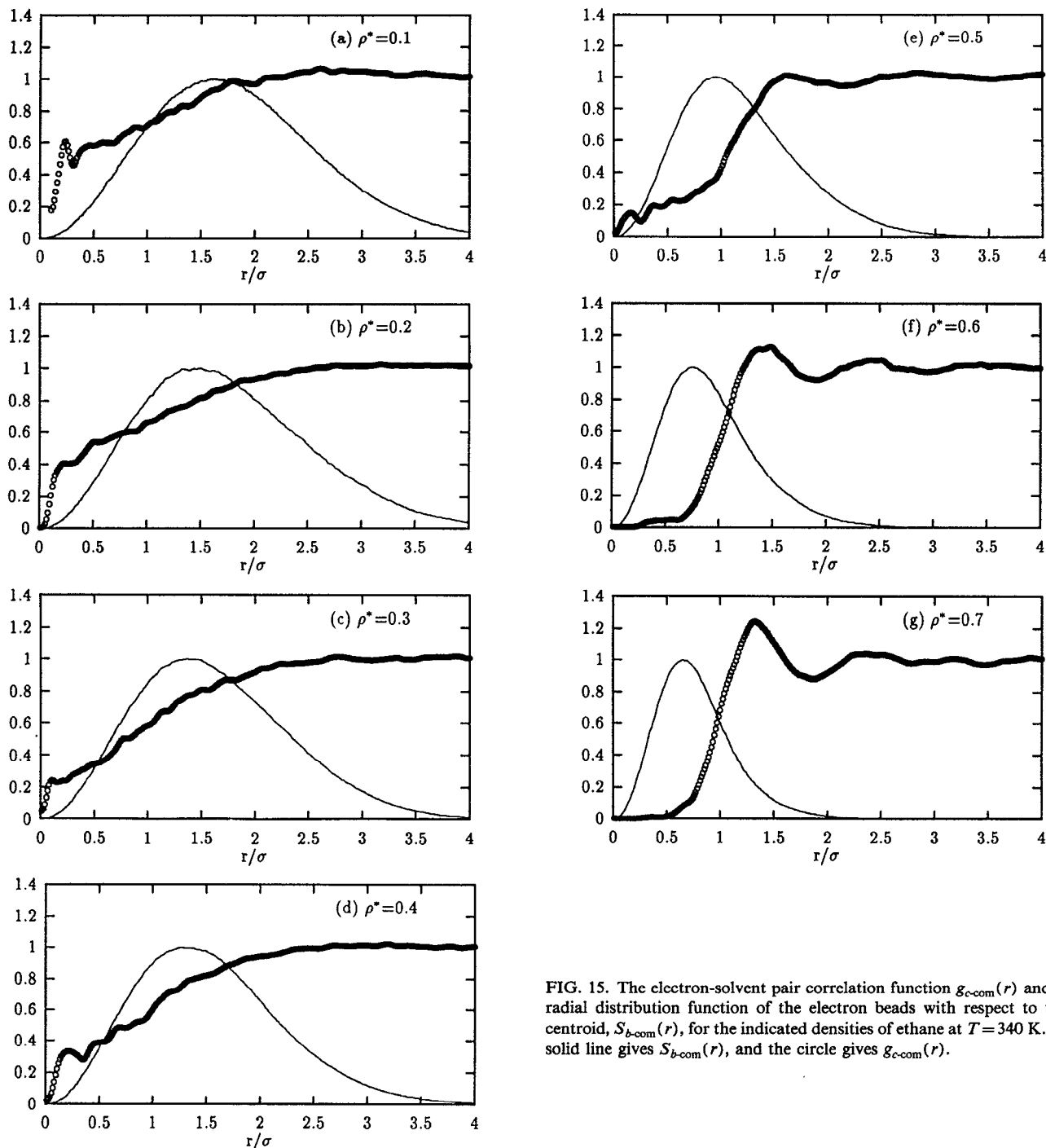


FIG. 15. The electron-solvent pair correlation function  $g_{e-com}(r)$  and the radial distribution function of the electron beads with respect to their centroid,  $S_{b-com}(r)$ , for the indicated densities of ethane at  $T = 340$  K. The solid line gives  $S_{b-com}(r)$ , and the circle gives  $g_{e-com}(r)$ .

increasing fluid density, but the kinetic energy begins to increase at a much faster rate than the decreasing rate of the potential energy. As will be seen later, the excess electron is localized in a cavity at high solvent densities and, therefore, the kinetic energy quickly increases as the size of the cavity decreases with increasing fluid density.

As in the methane study, we have studied how an electron perturbs solvent structure by calculating the ground state energy of an electron in the neat fluid and in the relaxed fluid. Figure 11 displays the density dependence of the electronic ground state energy in neat solvent configurations and in electron-equilibrated solvent configurations

generated from PIMC. As in methane, the excess electronic energies are calculated using the FFT-Lanczos method. It can be seen that there are very small energy differences between neat and relaxed fluids at  $\rho^* = 0.2, 0.3,$  and  $0.4$ , indicating that the solvated electron did not induce large scale reorganization in the solvent at these densities (as in methane). At reduced densities  $\rho^* > 0.5$ , there is a large energy difference between neat and relaxed fluids and the magnitude of the energy difference increases with density. The large energy difference indicates that the excess electron induces a large structural reorganization of ethane in marked contrast to what happens in methane.

We have also observed this type of behavior in the electron-He systems at high He densities where the electron induces a cavity in the solvent.<sup>26</sup>

Figure 12 gives the density dependence of the imaginary time correlation function,  $\mathcal{R}(\tau)$  [cf. Eq. (3.9)], of the electron in ethane. At low fluid densities (0.1 and 0.2), the  $\mathcal{R}(\beta\hbar/2)$  value is very close to the free particle value, and the  $\mathcal{R}(\tau)$  curves are parabolic. At high densities (above 0.5),  $\mathcal{R}(\beta\hbar/2)$  is much smaller than the free particle value and the  $\mathcal{R}(\tau)$  curves are flat at larger  $\tau$ . At intermediate solvent densities, the value of  $\mathcal{R}(\beta\hbar/2)$  lies between the free particle and the small high density values. In this intermediate density regime, the  $\mathcal{R}(\tau)$  curves are neither parabolic nor flat at large  $\tau$  and the value of  $\mathcal{R}(\beta\hbar/2)$  is found to fluctuate between large values characteristic of an extended state and small values characteristic of localized or self-trapped states. It is interesting to see how this behavior is reflected in the radial distribution of the electron beads around their centroid, as given by the distribution function  $S_{b\text{-com}}(r)$ . Figure 13 displays the density dependence of  $S_{b\text{-com}}(r)$ . At low densities, the  $S_{b\text{-com}}(r)$  curves are very close to that of a free electron. As the solvent density is increased, the peak of  $S_{b\text{-com}}(r)$  is shifted inward and becomes sharper and higher. At reduced densities above 0.5, the peaks have twice the height of the free particle at a much smaller  $r$ , about half the distance of the free particle peak. It is evident that the isomorphous electron polymer chain is more and more compressed as the solvent density increases. There is a dramatic change at  $\rho^*=0.5$ , above which the polymer chains wrap and fold into much smaller sizes and show significantly different behavior from that of the free electron.

The electron-carbon radial distribution function,  $g_{e-c}(r)$ , is presented as a function of the density in Fig. 14. The distance of closest approach of the electron to the carbon atom is about 0.82 Å (0.21 $\sigma$ ) and is independent of the fluid density. As also observed in electron solvation in methane, there is a nonmonotonic density dependence of the initial rise of the  $g_{e-c}(r)$ . At high ethane densities (0.5 and 0.7),  $g_{e-c}(r)$  has no evident peak structure, and for  $r < 3\sigma$   $g_{e-c}(r)$  is always less than 1, indicating that the electron is localized in a well defined cavity. At low density  $\rho^*=0.1$ ,  $g_{e-c}(r)$  does not exhibit a broad first peak as was seen in low density methane, indicating that the electron is not located on an ethane cluster.

The radial distribution function,  $g_{c\text{-com}}(r)$ , between the carbon atom and the com of the isomorphous electron polymer is displayed in Fig. 15; together with the radial distribution function of the electron beads with respect to their centroid,  $S_{b\text{-com}}(r)$  (normalized to have a peak value of unity). At low densities the peak positions of  $S_{b\text{-com}}(r)$  are located around 1.5 $\sigma$  and it can be seen that a significant fraction of the electron beads extend into the solvent without strongly perturbing the solvent density, except at distances close to the COM of the isomorphous electron polymer, but even near the com there is a finite fluid density. As the ethane density is increased, the peak in  $S_{b\text{-com}}(r)$  shifts toward the centroid of the electron and narrows and solvent atoms move away from the electron centroid. It is

clear that above a density of 0.5 the electron is localized in a solvent cavity. When  $g_{c\text{-com}}(r)$  begins to exhibit well defined first and second neighbor peaks, the first neighbor peak is already outside of the region where most of the electron beads reside. This is consistent with an increasingly localized electron, one that excludes solvent from the region that it occupies. At  $\rho^*=0.7$ , the cavity has a radius about 1.3 $\sigma$  (or 5.1 Å) and about 90% of electron beads are inside the cavity. The beads outside extend only to 2 $\sigma$  at most.

### C. Ethane: Two-site models

We studied two different two-site models of ethane to determine if it will be possible to describe the alkane data with a two site model.

(i) A simple site-site model in which the methyl and methylene groups are represented by soft spheres of diameter  $d$  for the repulsive cores seen by the electron and diameter  $\sigma$  for repulsive cores seen by other methyl and methylene groups. The electron-site potential is taken to be a WCA truncated LJ potential,<sup>28</sup>

$$V(r) = 4A[(d/r)^{12} - (d/r)^6] + A, \quad (4.1)$$

where  $A=6000$  K and  $d$  is the LJ radius of this potential (the potential energy is 6000 K at  $d$ ). The continuity of this potential makes it easier for simulation study than the hard sphere potential. The excess electron solvation in methane and ethane is simulated by the PIMC simulations with various  $d$  parameters and various fluid densities at  $T=340$  K. These simulations are found to give excellent agreement with hard sphere simulations and with the RISM-polaron theory for spherical methane.<sup>29,10</sup> When we performed simulations with  $d_{\text{methane}}=d_{\text{ethane}}=d$  it was found that, for the largest value of  $d=0.30\sigma$  that gives an extended electronic state in methane for  $0.9 \gg \rho^* > 0.1$ , the electron will also be in an extended state in ethane at  $\rho^*=0.6$  which is a very high fluid density for ethane. This is in marked disagreement with experiment. We find that this simple model gives the same qualitative behavior of the excess electron in methane as in ethane. However, by choosing  $d_{\text{methane}}=0.30\sigma$  and  $d_{\text{ethane}}=0.38\sigma$ , we can obtain agreement with the experiment. However, then it will be difficult to extend this model to large branched and chain alkanes. We infer from this that the simple two site RISM polaron type model with  $d_{\text{methane}}=d_{\text{ethane}}$  will be a poor model for the alkane fluids.

(ii) We studied a two site model with  $A_3=0$  in Eq. (2.2), a model in which the repulsive site centered on the C-C bond is omitted with PIMC, and found that the excess electron behaves the same in ethane as it does in methane. It forms an extended state over a wide density regime in contradiction with experiment.

## V. DISCUSSION

The central focus of this paper has been to ascertain the difference in the solvation properties of excess electrons in the two simplest hydrocarbon fluids. Pseudopotentials

representing the interaction between an electron and methane and ethane were devised. These electron-methane pseudopotentials fitted from scattering data reproduce the experimental density dependence of the threshold to photoemission  $V_0$  only when many-body polarization interactions are included. In the ethane pseudopotential an additional repulsive site is placed at the midpoint of the C–C bond. The quantitative differences between the experimentally measured zero-field electron mobility in fluid methane and ethane can be understood qualitatively in terms of these pseudopotentials. Simulations show that if the repulsive center on the C–C bond is omitted from ethane an excess electron will behave in ethane as it does in methane, that is, it will form an extended state over a wide density regime in contradiction with experiment. This study clearly shows that such terms in the pseudopotential might be important in explaining why in branched hydrocarbons an excess electron forms extended high-mobility states, whereas in chain alkanes, like *n*-alkanes, they form localized or self-trapped states. Indeed, it was to gain such insight that we chose first to study these simple fluids. In a subsequent publication we will present results on a comparison between neopentane and *n*-pentane which clearly show that the C–C repulsive site also gives agreement with observation.

We have found that a simple site–site pseudopotential based only on methylene sites (thus ignoring the additional repulsive bond site) will not be able to account for the morphological differences between chain and branched molecules unless one sacrifices the requirement of transferability.

Our simulations show that electron solvation in methane is very similar to electron solvation in Xe.<sup>8,9</sup> The excess electron is in an extended state throughout the whole solvent densities studied ( $0.1 \leq \rho^* \leq 0.9$ ). At low methane density ( $\rho^* = 0.1$ ), the electron is found to be in an extended state. The local solvent structure around the solvated electron reveals that the excess electron resides on clusters of solvent molecules with a higher density than the uniform solvent density. This is because these higher density clusters provide a network of deep attractive channels which will reduce the electronic potential energy. This phenomenon has also been observed in electron solvation in Xe by Coker *et al.*<sup>8</sup> and in electron solvation in Xe clusters by Martyna *et al.*<sup>20</sup> Low density regions surrounding the clusters act as potential barriers and prevent electron motion from one cluster to another. The electron is thus trapped at low densities by a cluster of methane molecules arising from solvent density fluctuations. The corresponding condensed phase Ramsauer–Townsend picture is that the electron experiences an effective repulsion from the surrounding solvent. At intermediate methane densities ( $\rho^* = 0.3, 0.5, \text{ and } 0.7$ ), it is observed that the solvated excess electron does not perturb the local solvent density and the electronic ground state energy is almost identical to that in the neat fluid. The solvated electron is found to be in an extended state without much compression from the surrounding solvent molecules. The attractive potential

energy channels are broad and extend throughout the solvent, allowing for percolation of the excess electron without much resistance. This corresponds to a Ramsauer–Townsend picture in which the electron does not experience any net interaction or “force” from the surrounding solvent configurations and thus sees an almost transparent media. Since the simulations were performed at a supercritical temperature, we have been able to study a much wider density regime of this fluid which supports high mobility electron states. When the solvent density reaches  $\rho^* = 0.9$ , the solvated electron is compressed by the solvent but nevertheless still extends into the solvent. The attractive potential channels become narrower and less attractive so that the repulsive potential becomes more important. To reduce the electronic energy, the excess electron favors solvent configurations of lower density which has wider and deeper attractive potential channels. The electron wave function is compressed because of the resistance to density change in the surrounding solvent. The high density solvent configurations with narrow channels separating low density regions with wide and deep channels provide energy barriers to electron percolation. This picture is consistent with the condensed phase Ramsauer–Townsend effect. When integrating over the volume occupied by the electron, there is a net repulsive interaction due to the narrow channels in the surrounding higher density solvent configurations. Therefore, there should be a drop in the electron mobility as the solvent density increases from  $\rho^* = 0.7$  to 0.9 in agreement with the experimentally observed abrupt mobility drop after the mobility maximum.

In ethane, the experimental density dependence of the electron zero-field mobility suggests that there is a transition from a delocalized state to a localized (self-trapped) state as the ethane density increases.<sup>30</sup> Our simulations also exhibit a transition from delocalized to localized electronic states with increasing solvent density. At low ethane densities, the solvated electron is in an extended state resembling a free electron at the same temperature, and there is no indication that the solvated electron resides in high density regions in the solvent. The electron has a lower ground state energy in electron equilibrated solvent configurations than in neat solvent configurations, indicating that there may be a reorientation of the ethane molecules near the electron due to the anisotropic electron-ethane interaction potential. At this low density, the ethane molecules are relatively free to rotate to reduce the energy of the solvated electron, and provide open channels for the electron to percolate. As the ethane density increases from  $\rho^* = 0.2$ –0.4, the solvated electron can still be characterized as being in an extended state extending almost as far as that of a free electron and the electron polymer chain has a large radius of gyration  $R(\beta\hbar/2)$ . The region where the solvated electron resides has a slightly lower ethane density than the bulk solvent density, but there is no evident energy difference between the electronic ground state energies in the neat and electron equilibrated configurations thus indicating that the electron does not induce solvent reorganization. At these intermediate densities, the solvated electron while still in an extended state is also slightly trapped by

the solvent density fluctuations. Due to the anisotropy of the electron-ethane interaction, the repulsive bulge on the C-C bond obstructs the formation of attractive potential channels in the solvent. The excess electron thus favors lower density ethane configurations where the molecules can be easily rotated to form deep continuous channels. The stronger intermolecular interaction at higher densities hinders the rotation of ethane molecules and thus makes it difficult for the electron to find a continuous network through which to percolate. With this effect, the electron mobility decreases with increasing ethane density. At densities higher than 0.5, the electron is found in a localized state becomes ground state dominated. The solvated electron reorganizes the solvent and becomes self-trapped. At these densities, the bond centered repulsions begins to cut off the attractive channels, making the formation of a cavity more energetically favorable. This was demonstrated by the larger energy differences between the electronic ground state energies in the neat and relaxed solvent configurations as the ethane density increases from  $\rho^* = 0.5$ –0.7. The non-existence of continuous attractive potential channels in the high density solvent prevents the electron from percolating. The temperature dependence of the electron mobility in ethane shows that electron conduction is an activated process with activation energies of approximately 0.1 eV,<sup>31</sup> a value very close to our calculated electronic ground state energy difference between the neat and relaxed solvent configurations (they are 0.04, 0.08, and 0.20 eV for  $\rho^* = 0.5$ , 0.6, and 0.7, respectively). In the condensed phase Ramsauer-Townsend interpretation, this corresponds to the fact that the electron experiences a strong net repulsion from the surrounding solvent.

In conclusion, we find the following.

The excess electronic state in methane is extended throughout the whole density regime studied. This system resembles Xe.<sup>8,9</sup>

A simple two site pseudopotential model of the electron ethane interaction (with the sites centered on the C atoms) predicts that the electron will be found in an extended state in ethane as in methane over the whole density regime simulated in marked disagreement with experiment. This model gives rise to deep attractive channels through which the electron can percolate and is inconsistent with experiment. A simple two site RISM polaron model also predicts that the electron will be found in extended states in both methane and ethane throughout the density regime studied again in marked disagreement with experiment. We could not devise a simple two site model that gives a consistent prediction of the observed differences between electron solvation in ethane and methane and that has the property of portability to other branched and chain alkanes.

A simple three site pseudopotential model of the electron ethane interaction with a repulsive site at the bisector of the C-C bond is consistent with experiment in that at low fluid densities the electron is found to be in an extended state but at higher fluid density the electron becomes self-trapped.

The previous observations lead to a possible explanation

of why electrons are highly mobile in methane and not in ethane. In methane at high density a contiguous network of attractive channels can exist through which the excess electron can percolate (as in fluid Xe). These channels are due to the electron molecule attractions arising from many-body polarization interactions. In ethane at high density the repulsive site on the C-C bonds blocks these attractive channels and prevents the electron from percolating.

The same mechanism should come into play in other fluids like *n*-pentane and neopentane and explains why in branched hydrocarbons the electron is highly mobile but in chain hydrocarbons it is self-trapped. Simulations of these more complex fluids will be published in a subsequent paper.

## ACKNOWLEDGMENTS

We wish to thank Dr. Glenn Martyna for useful discussions and for critically reading the manuscript. This work was supported by a grant from the National Science Foundation (NSF CHE-91-22-506) and by a grant of supercomputer time from NCSA at the University of Illinois, Urbana.

- <sup>1</sup>R. A. Holroyd and W. F. Schmidt, *Annu. Rev. Phys. Chem.* **40**, 439 (1989).
- <sup>2</sup>W. F. Schmidt, *IEEE Trans. Elect. Insul.* **19**, 389 (1984).
- <sup>3</sup>W. F. Schmidt, *Can. J. Chem.* **55**, 2188 (1977).
- <sup>4</sup>J. Jortner and A. Gaathon, *Can. J. Chem.* **55**, 1801 (1977).
- <sup>5</sup>D. F. Coker and B. J. Berne, in *Excess Electrons in Dielectric Media*, edited by Jean-Paul Jay-Gerlin and C. Ferradini (CRC Press, Boca Raton, 1991), pp. 211–257.
- <sup>6</sup>I. György and G. R. Freeman, *J. Chem. Phys.* **70**, 4769 (1979).
- <sup>7</sup>K. Nakagawa, K. Itoh, and M. Nishikawa, *IEEE. Trans. Elect. Insul.* **23**, 509 (1988).
- <sup>8</sup>D. F. Coker, B. J. Berne, and D. Thirumalai, *J. Chem. Phys.* **86**, 5689 (1987).
- <sup>9</sup>B. Space, D. F. Coker, Z. H. Liu, B. J. Berne, and G. Martyna, *J. Chem. Phys.* **97**, 2002 (1992).
- <sup>10</sup>D. L. Laria and D. Chandler, *J. Chem. Phys.* **87**, 4088 (1987).
- <sup>11</sup>U. Asaf, R. Reininger, and I. T. Steinberger, *Chem. Phys. Lett.* **100**, 363 (1983).
- <sup>12</sup>Y. Yamaguchi, T. Nakajima, and M. Nishikawa, *J. Chem. Phys.* **71**, 550 (1979).
- <sup>13</sup>U. Asaf and I. T. Steinberger, *Chem. Phys. Lett.* **128**, 91 (1986).
- <sup>14</sup>R. Reininger, U. Asaf, and I. T. Steinberger, *Chem. Phys. Lett.* **90**, 287 (1982).
- <sup>15</sup>A. Jain, *Phys. Rev. A* **34**, 954 (1986).
- <sup>16</sup>J. Yuan, *J. Phys. B* **21**, 3113 (1988).
- <sup>17</sup>J. Yuan (private communication).
- <sup>18</sup>Z. H. Liu and B. J. Berne (in preparation).
- <sup>19</sup>J. O. Hirschfelder, C. F. Curtiss, and R. B. Bird, *Molecular Theory of Gases and Liquids* (Wiley, New York, 1954).
- <sup>20</sup>G. J. Martyna and B. J. Berne, *J. Chem. Phys.* **88**, 4516 (1988).
- <sup>21</sup>R. P. Feynman, *Statistical Mechanics* (Benjamin, New York, 1972).
- <sup>22</sup>E. L. Pollock and D. M. Ceperley, *Phys. Rev. B* **30**, 2555 (1984).
- <sup>23</sup>A. L. Nichols, D. Chandler, Y. Singh, and D. M. Richardson, *J. Chem. Phys.* **81**, 5109 (1984).
- <sup>24</sup>J. K. Cullum and R. A. Willoughby, *Lanczos Algorithms for Large Symmetric Eigenvalue Computations* (Birkhauser, Boston, 1985).
- <sup>25</sup>F. Webster, P. J. Rossky, and R. A. Friesner, *Comput. Phys. Commun.* **63**, 494 (1991).
- <sup>26</sup>Z. H. Liu and B. J. Berne (unpublished). The FFT-Lanczos method was used to calculate the electronic ground state energy in both neat and electron equilibrated He and Xe configurations. The electron equilibrated solvent configurations were generated by the Coker *et al.* PIMC

simulation of electron solvation in He (Ref. 8) and Xe (Ref. 5). It was found that the electron is delocalized in Xe but localized in high density He.

<sup>27</sup>J. A. Barker and R. O. Watts, *Chem. Phys. Lett.* **3**, 144 (1973).

<sup>28</sup>J. D. Weeks, D. Chandler, and H. C. Andersen, *J. Chem. Phys.* **54**, 5237 (1971).

<sup>29</sup>M. Sprik, M. L. Klein, and D. Chandler, *J. Chem. Phys.* **83**, 3042 (1985).

<sup>30</sup>W. Döldissen, W. F. Schmidt, and G. Bakale, *J. Phys. Chem.* **84**, 1179 (1980).

<sup>31</sup>M. G. Robinson and G. R. Freeman, *Can. J. Chem.* **52**, 440 (1974).